Impacts of nodal demand allocations on transient-based skeletonization of water distribution systems

Yuan Huang, Feifei Zheng*, Huan-Feng Duan, M. ASCE, Qingzhou Zhang and Yonggang Shen

Yuan Huang: Postdoctoral fellow, College of Civil Engineering and Architecture, Zhejiang University, 866 Yuhangtang Rd, Hangzhou, China 310058. yuanhuangzju@zju.edu.cn

Feifei Zheng: Corresponding author, Professor, College of Civil Engineering and Architecture, Zhejiang University, 866 Yuhangtang Rd, Hangzhou, China 310058. feifeizheng@zju.edu.cn

Huan-Feng Duan: Associate Professor, Department of Civil and Environmental Engineering, The Hong Kong Polytechnic University, Hung Hom, Kowloon, 999077, Hong Kong. hf.duan@polyu.edu.hk

Qingzhou Zhang: Postdoctoral fellow, College of Civil Engineering and Architecture, Zhejiang University, 866 Yuhangtang Rd, Hangzhou, China 310058. wdswater@gmail.com

Yonggang Shen: Associate Professor, College of Civil Engineering and Architecture, Zhejiang University, 866 Yuhangtang Rd, Hangzhou, China 310058. sygdesign@zju.edu.cn

Abstract: Urban water distribution systems (WDSs) are often skeletonized to enable efficient system analysis and management. While different methods are available to account for transient dynamics within the skeletonization processes, they often ignore the potential impacts induced by nodal demand allocations. This paper proposes a transient-based method to skeletonize pipes in series with internal demands, where the optimal demand allocation strategy is determined by a minimization approach associated with a probabilistic evaluation method. In addition, this paper makes the first attempt to investigate the impacts of different nodal demand allocation strategies on reproducing transient dynamics within the skeletonization process. The proposed method is demonstrated for a hypothetic transmission system and a realistic WDS. Results show that (i) the impact of demand allocations on transient dynamics is positively correlated with demand values; and (ii) the proposed skeletonization method overall outperforms the traditional methods in capturing the transient dynamics of the original WDS, especially for nodes with relatively large demands.

Authors' Keywords: water distribution systems (WDSs); skeletonization; transient; pipes in series; nodal demand.

Introduction

Water distribution system (WDS) models have been widely used by water utilities for a range of purposes including system planning, operation and management (e.g., Walski 1984; Kapelan et al. 2007; Zheng et al. 2016; Zheng et al.2017; Zhang et al. 2018). To develop such WDS models, geographic information systems (GISs) have been often employed to provide network topology and physical attributes of the hydraulic components (e.g., pipes, junctions and valves) (Walski et al. 2004; Jung et al. 2007). While being able to exhibit comprehensive information of the system, WDS models taken from GIS are often very complex in structure and topology, with pipes/nodes up to hundreds of thousands (Deuerlein 2008). This may result in significant challenges/difficulties for system simulation, management and operation. Consequently, WDS models abstracted from GISs or other data sources are often skeletonized to reduce their scales/complexities, aimed to enable efficient system modeling and analysis (Walski et al. 2003; Hellbach et al. 2011).

In the literature, many methods are available to skeletonize WDS models, including branch trimming, node aggregations, merging of pipes and removals of non-essential components (Walski et al. 2003; Jung et al. 2007). These skeletonization methods are mainly developed based on steady-state hydraulic equivalence (mass and energy conservations), i.e., the head losses through the skeletonized pipes/nodes should be overall similar to those of the original system (Walski et al. 2003; Saldarriaga et al. 2008). These resultant WDS models can reproduce similar steady-state hydraulic performance with the original systems, enabling wider up-take of skeletonized models for practical applications (Perelman and Ostfeld 2011).

While the methods mentioned above have made significant progress and contributions in skeletonizing WDS models, they mostly consider the model skeletonization under steady-state hydraulic conditions. This implies that the performance of the skeletonized models in capturing transient dynamics of the original systems remains unknown (Gad and Mohammed 2014) as these steady-stated based methods typically ignore the interaction and attenuation of transient pressure waves within the skeletonization process (Duan and Lee 2015; Meniconi et al. 2015). To address this issue, attempts have been made to assess the performance of the skeletonized models in reproducing the transient behaviour of the original system (Martin 2000). The results showed that the skeletonized models based on steady-state hydraulic conditions may introduce substantial errors for the transient response of WDSs (Jung et al. 2007; Meniconi et al. 2018; AWWA 2019), especially when the nodes with larger water demands or high elevations are skeletonized (Walski et al. 2004). This may lead to large potential risk when using these skeletonized WDS models to manage extreme events induced by transients (e.g., pipe bursts) or design transient-defensed hydraulic infrastructures (Boulos et al. 2005; Ebacher et al. 2011; Rathnayaka et al. 2016).

While large transient dynamic deviations between the skeletonized WDS models produced by the steady-state based methods and the original systems are acknowledged, there have been surprisingly few efforts made to develop skeletonization methods with transient dynamics explicitly considered. A recent study conducted by Huang et al. (2019) introduced a transient-based method for the skeletonization of series pipes with no internal demands, aimed to deal with the dummy nodes (i.e. nodes with no demands) of the WDSs that are often used to represent joints between different pipe diameters/configurations and connections

between different hydraulic elements. The results from Huang et al. (2019) showed that their method significantly outperforms the traditional steady-state based method in reproducing the transient behavior of the original systems. However, their proposed method cannot be applied to pipes with internal demands. This limitation has significantly hampered the wide up-take of their method (Huang et al., 2019) for many practical applications as plenty of pipes are associated with demand nodes (representing water consumptions by the users) in the WDS.

To our best knowledge, there is so far no method available that can be used to skeletonize the pipes in series with internal demands (denoted as PSIDs for simplicity in this study, i.e., pipes in series with intermediate demand nodes). In addition, there is a lack of understanding for the impacts of different demand allocations within the skeletonization process on mimicking the transient dynamics of the WDS models. More specifically, it is unknown to what extent the different nodal demand allocation strategies can affect the transient dynamics of the WDS models; how these impacts are influenced by the amounts of nodal demands; and how important of the transient impacts induced by nodal demand allocations relative to those caused by the adjustments of pipe attributes within the skeletonization process.

To address the gaps outlined above, this paper aims to: (i) develop a generic transient-based skeletonization approach that is able to handle PSIDs for the WDS models; and (ii) provide investigation and analysis on the transient behaviors induced by demand allocations within the skeletonization process of WDSs. It is anticipated that this paper not only provides a transient-based method to optimally allocate nodal demands within the pipe skeletonization process, but also builds knowledge regarding the underlying properties of the resultant transient dynamics caused by demand

allocations.

Methodology

A generic transient-based method is firstly developed to skeletonize the pipes in series with internal demands (PSIDs). This is followed by intensive numerical experiments designed to investigate the impacts of nodal demand allocations on transient dynamics within the skeletonization process. Three traditional skeletonization approaches are also used to compare with the proposed method in reproducing the transient dynamics of the original systems. Two assessment metrics are defined to quantitatively evaluate the performance of the skeletonized systems.

Generic transient-based skeletonization method for PSIDs

For transient-based skeletonization, two accuracy control criteria (i.e., the phase criterion and the amplitude criterion) are often used to ensure the travelling time and amplitude of pressure waves through the skeletonized systems as close as those in the original WDS (Huang et al. 2019). These two criteria are also considered as principles of the proposed method in this paper. Within the proposed method, a two-step skeletonization procedure is combined with a probabilistic method to quantify nodal demand effects on transient dynamics. In addition, two optimization objectives are proposed to minimize the skeletonization errors induced by the internal demand allocation and the merging of pipes in series respectively. More specifically, the internal nodal demand of a PSID is allocated to two end nodes with an optimal allocation coefficient with the aid of the proposed probabilistic approach in Step 1. This is followed by merging these pipes in series into one simple pipeline with optimal equivalent attributes (i.e., the length, wave speed, diameter and friction factor

of the pipe) in Step 2.

Fig. 1(a) shows a typical system of pipes in series, which is used to illustrate the proposed method. This simple system consists of four pipes (P_1, P_2, P_3, P_4), two end nodes (N_1, N_2), and an internal node N_3, where all these three nodes N_1, N_2 and N_3 have demands (q_1, q_2 and q_3 in Fig. 1a). For Step 1, the demand of N_3 is optimally allocated to the two end nodes N_1 and N_2 with an allocation coefficient r (i.e., weighting factor) by minimizing the skeletonization error induced by the internal demand allocation, so that the demands of N_1 and N_2 increase to $q_1 + rq_3$ and $q_2 + (1-r)q_3$ respectively (Fig. 1b). In Step 2, pipes P_1 and P_2 are merged into an equivalent pipe P_e (Fig. 1c), with maintaining the steady-state equivalence and minimizing the skeletonization error induced by the merging of series pipes. Details of the proposed two-step skeletonization method and the adopted probabilistic evaluation approach are elaborated as follows.

Step 1: Nodal demand allocation for WDS skeletonization

Within Step 1 of the proposed method, demands of N_3 are optimally allocated to N_1 and N_2, in order to minimize the transient modeling errors introduced by skeletonization following the amplitude criterion. That is, the pressure wave transformations at two end nodes N_1 and N_2 in the skeletonized system (Fig. 1b) should be as close as those in the original system (Fig. 1a). Assuming a pressure wave with amplitude Δh traveling from P_3 through N_1 in the original system (Fig. 1a), the pressure change (or the amplitude of the transmitted wave) can be calculated based on the wave transformation equation at the node boundary (Huang et al. 2017; Wood et al. 2005), as

$$\Delta h^{P_3\to N_1} = \Delta h_p^{P_3\to N_1} - \Delta h_q^{P_3\to N_1} = \left(1-\Psi^{P_3\to N_1}\right)\Delta h_p^{P_3\to N_1} \quad (1)$$

where $\Delta h_p^{P_3\to N_1} = T^{P_3\to N_1}\Delta h$ represents the transient pressure change due to the transformation of the incident wave travelling from P_3 through N_1 without considering the nodal demand impact, which is defined herein as the pseudo pressure change; $T^{P_3\to N_1} = \left(2/B_3\right)\Big/\sum_{m=1}^{M}\left(1/B_m\right)$ is the transmission coefficient for the incident wave traveling from P_3 through N_1 (Chaudhry 2014), in which M is the total number of connected pipes at N_1, $B = a/(gA)$ is the characteristic impedance of the pipe (Gong et al. 2018) with a as the wave speed, A as the pipe cross-sectional area, and g as the gravitational acceleration; $\Delta h_q = \Delta q\Big/\sum_{m=1}^{M}\left(1/B_m\right)$ represents the pressure change resulting from the change of the nodal demand, which is defined as the nodal demand disturbance; Δq denotes the change of the nodal demand due to the change of the transient pressure head during the wave transformation at the node; $\Psi = \Delta h_q/\Delta h_p$ is the ratio of the nodal demand disturbance to the pseudo pressure change, which is used to represent the nodal demand effect.

The relation between nodal demand and transient pressure head is generally taken as (Jung et al. 2007; Ebacher et al. 2011)

$$q = C_q H^{\alpha} \quad (2)$$

where q is the nodal demand; H is the pressure head representing the total head minus the nodal elevation; C_q is the equivalent orifice emitter coefficient of nodal demand and α is an exponential index ($\alpha = 0.5$ is usually used). The coefficient C_q is determined from the initial steady-state condition, i.e., $C_q = q_0/H_0^{\alpha}$ where q_0 and H_0

are the initial nodal demand and pressure head respectively. Substituting this pressure-driven demand into Eq. (1), the nodal demand effect can be defined as

$$\Psi^{P_3 \to N_1} = S^{N_1} \frac{\left(H^{N_1} + \Delta h^{P_3 \to N_1}\right)^{\alpha} - \left(H^{N_1}\right)^{\alpha}}{\Delta h_p^{P_3 \to N_1}} \tag{3}$$

where $S^{N_1} = C_q^{N_1} \Big/ \sum_{m=1}^{M} \left(1/B_m\right)$ represents the integrated term associated with the initial steady-state condition and the pipe attributes at N_1, which are all static relative to the dynamic transient status, thus it is defined as the static attribute; H^{N_1} is the transient pressure head at N_1 before the transformation of the incident wave, thus is defined as the previous pressure. Eq. (3) shows that the nodal demand effects on transient dynamics (i.e., Ψ) are time- and event-dependent during transient processes as the two relevant parameters (i.e., the previous pressure H and the pseudo pressure change Δh_p) are highly dynamic in time evolutions and transient events, thus it cannot be explicitly quantified prior to a specific transient analysis. To address this issue, a probabilistic approach based on Monte-Carlo simulation (MCS) is proposed to explicitly evaluate the effects of nodal demands on transient dynamics from the probability perspective.

The proposed probability approach is achieved by utilizing the MCS method for the nodal demand effect (Ψ) regarding the two dynamic parameters, i.e., the pseudo pressure change Δh_p and the previous pressure H. A total of 100,000 MCS runs are conducted for each of different static attributes (S) to obtain sufficient results for statistical analysis (Duan et al. 2011). For demonstration, Fig. 2(a) plots the probability density functions (PDFs) of nodal demand effect (Ψ) for three different static attributes (S = 20, 50 and 100 $m^{0.5}$). It is observed that the distribution of Ψ is

206 concentrated in a relatively limited range, with overall larger values of Ψ associated
207 with greater values of static attribute. This suggests that the two dynamic parameters
208 (H and Δh_p) have limited impacts on Ψ, which agrees well with the findings
209 reported in Huang et al. (2017). Fig. 2(b) presents the maximum probability and
210 expectation of the PDFs across different static attributes (S). Monotonically increasing
211 functions between the statistical parameters and the static attribute of the node can be
212 observed from this figure. Results in Fig. 2 imply that the degree of the nodal demand
213 effect (Ψ) can be approximately estimated using derived relationships between Ψ
214 and nodal static attributes as shown in Fig. 2(b). Accordingly, a probability-based
215 parameter ($\widetilde{\Psi}^{N_1}$) relevant to the static attribute (S^{N_1}) at N_1 is used to represent the
216 dynamic nodal demand effect ($\Psi^{P_3\to N_1}$) in Eq. (3).

217 With this probabilistic approach, taking again the case in Fig. 1 for example, the wave
218 transformations at the two end nodes N_1 and N_2 can be analyzed by following the
219 amplitude criterion. Assuming that a pressure wave with amplitude Δh travels from
220 Pipe P_3 to Pipe P_4, the wave transformations at two end nodes N_1 and N_2 resulted
221 from the first impinging of the pressure wave on the two nodes can be estimated
222 respectively, as follows

223 (a) The wave transformation before the demand allocation (Fig. 1a),

224 $$\Delta h_0^{P_3\to N_1} \approx \left(1-\widetilde{\Psi}_0^{N_1}\right) T_0^{P_3\to N_1}\Delta h \tag{4}$$

225 $$\begin{aligned}\Delta h_0^{P_3\to N_2} &\approx \Delta h_0^{P_3\to N_1}\Delta h_0^{P_1\to N_3}\Delta h_0^{P_2\to N_2}\\ &\approx \left(1-\widetilde{\Psi}_0^{N_1}\right)\left(1-\widetilde{\Psi}_0^{N_3}\right)\left(1-\widetilde{\Psi}_0^{N_2}\right) T_0^{P_3\to N_1} T_0^{P_1\to N_3} T_0^{P_2\to N_2}\Delta h\end{aligned} \tag{5}$$

226 (b) The wave transformation after the demand allocation (Fig. 1b),

227 $$\Delta h_d^{P_3\to N_1} \approx \left(1-\widetilde{\Psi}_d^{N_1}\right) T_d^{P_3\to N_1}\Delta h \tag{6}$$

228
$$\begin{aligned}\Delta h_d^{P_3\to N_2} &\approx \Delta h_d^{P_3\to N_1}\Delta h_d^{P_1\to N_3}\Delta h_d^{P_2\to N_2}\\ &\approx \left(1-\widetilde{\Psi}_d^{N_1}\right)\left(1-\widetilde{\Psi}_d^{N_2}\right)T_d^{P_3\to N_1}T_d^{P_1\to N_3}T_d^{P_2\to N_2}\Delta h\end{aligned} \tag{7}$$

229 where the subscripts 0 and *d* indicate the transient status of the original system and the
230 skeletonized system after the demand allocation, respectively. As the characteristic
231 impedances of pipes after demand allocation are not changed (i.e., $B_d = B_0$), the
232 transmission coefficients at all nodes are identical to those in the original system, i.e.,
233 $T_d = T_0$ for each node. The approximate signs in these equations is due to (i) the
234 probabilistic evaluation of nodal demand effects and (ii) other factors influencing the
235 propagation of pressure waves, such as the effects of friction, viscoelasticity and
236 vibration of the pipeline, which are generally considered to be insignificant for pipes
237 with relatively small length that are mainly considered for skeletonization in practice
238 (Walski et al. 2003).

239 Similarly, for a pressure wave travels from P_4 to P_3 (i.e., the opposite direction), the
240 wave transformations at two end nodes N_1 and N_2 can also be derived in similar forms.
241 Therefore, a weighted least squares optimization problem is formed to implement the
242 minimization approach for the amplitude criterion. That is, the differences of the wave
243 transformations at two end nodes between the original and skeletonized systems (i.e.,
244 Fig. 1a and b) from both traveling directions are simultaneously minimized to enable
245 global optima, which can be expressed as follows by eliminating Δh,

$$
\begin{aligned}
Min: \quad E_d = w_1 & \left\{ \begin{bmatrix} \left[\left(1-\widetilde{\Psi}_0^{N_1}\right)T_0^{P_3\to N_1} - \left(1-\widetilde{\Psi}_d^{N_1}\right)T_0^{P_3\to N_1}\right]^2 + \\ \left[\left(1-\widetilde{\Psi}_0^{N_2}\right)\left(1-\widetilde{\Psi}_0^{N_3}\right)\left(1-\widetilde{\Psi}_0^{N_1}\right)T_0^{P_4\to N_2}T_0^{P_2\to N_3}T_0^{P_1\to N_1} - \\ \left(1-\widetilde{\Psi}_d^{N_2}\right)\left(1-\widetilde{\Psi}_d^{N_1}\right)T_0^{P_4\to N_2}T_0^{P_2\to N_3}T_0^{P_1\to N_1} \end{bmatrix}^2 \right\} \\
& + w_2 \left\{ \begin{bmatrix} \left[\left(1-\widetilde{\Psi}_0^{N_2}\right)T_0^{P_4\to N_2} - \left(1-\widetilde{\Psi}_d^{N_2}\right)T_0^{P_4\to N_2}\right]^2 + \\ \left[\left(1-\widetilde{\Psi}_0^{N_1}\right)\left(1-\widetilde{\Psi}_0^{N_3}\right)\left(1-\widetilde{\Psi}_0^{N_2}\right)T_0^{P_3\to N_1}T_0^{P_1\to N_3}T_0^{P_2\to N_2} - \\ \left(1-\widetilde{\Psi}_d^{N_1}\right)\left(1-\widetilde{\Psi}_d^{N_2}\right)T_0^{P_3\to N_1}T_0^{P_1\to N_3}T_0^{P_2\to N_2} \end{bmatrix}^2 \right\}
\end{aligned} \tag{8}
$$

where E_d is the sum of weighted squared residuals, and a smaller value of E_d (i.e., approaching to zero) indicates less differences of the wave transformations between the original and skeletonized systems, thus it is considered as the indicator of the skeletonization error introduced by the internal demand allocation in this paper. The first term on the right-hand side represents the weighted sum of the differences of the pressure changes at N_1 between the original and skeletonized systems; the second term represents such a difference at N_2. The weights $w_1 = \left(L_1/A_1\right)/\left(L_1/A_1 + L_2/A_2\right)$ and $w_2 = 1 - w_1$ representing the relative difference in the initial fluid inertia between two series pipes are used to indicate the relative importance of the squared differences at two end nodes (Huang et al. 2019). Therefore, the solution of Eq. (8) yields the optimized r and the corresponding skeletonization error E_d for the demand allocation.

Step 2: Series pipes merging for WDS skeletonization

Using the above-mentioned demand allocation strategy, the internal demand of node N_3 has been moved to the end nodes (i.e., no internal demand for N_3 in Fig. 1b). Consequently, the transient-based method proposed by Huang et al. (2019) for the skeletonization of series pipes with no internal demand can be applied. That is, for step 2 of merging pipes in series (Fig. 1c), the two accuracy control criteria (i.e., transient phase criterion and the amplitude criterion) and the traditional hydraulic

equivalence theory are followed to enable the skeletonization. The following equations are used for this purpose.

$$\frac{L_e}{a_e} = \frac{L_1}{a_1} + \frac{L_2}{a_2} \tag{9}$$

$$\begin{aligned} Min: \quad E_s = w_1 & \left[\begin{aligned} & \left(T_0^{P_3 \to N_1} - T_s^{P_3 \to N_1}\right)^2 \\ & + \left(T_0^{P_4 \to N_2} T_0^{P_2 \to N_3} T_0^{P_1 \to N_1} - T_s^{P_4 \to N_2} T_s^{P_e \to N_1}\right)^2 \end{aligned} \right] \\ + w_2 & \left[\begin{aligned} & \left(T_0^{P_4 \to N_2} - T_s^{P_4 \to N_2}\right)^2 \\ & + \left(T_0^{P_3 \to N_1} T_0^{P_1 \to N_3} T_0^{P_2 \to N_2} - T_s^{P_3 \to N_1} T_s^{P_e \to N_2}\right)^2 \end{aligned} \right] \end{aligned} \tag{10}$$

$$\frac{L_e Q_e^{1.852}}{C_e^{1.852} D_e^{4.87}} = \frac{L_1 Q_1^{1.852}}{C_1^{1.852} D_1^{4.87}} + \frac{L_2 Q_2^{1.852}}{C_2^{1.852} D_2^{4.87}} \tag{11}$$

where L, a, D, C and Q are the length, wave speed, diameter, Hazen–Williams (H-W) coefficient and flow rate of the pipe respectively; subscripts 1, 2 and e represent pipes P_1, P_2 and P_e respectively; In Eq. (10), E_s is the sum of weighted squared residuals based on the defined weighted least squares approximation, thus it is considered as the indicator of the skeletonization error introduced by the merging of two series pipes; the subscript s indicates the transient status of the skeletonized system after the series pipe merging; the first term on the right-hand side represents the weighted sum of the differences of the pressure changes at N_1 between the skeletonized systems after the demand allocation and the series pipe merging; the second term represents such a difference at N_2.

Typically, the total length of the original pipes in series is taken as the equivalent length of the skeletonized pipeline (i.e., $L_e = L_1 + L_2$, Walski et al. 2003). Hence the wave speed of the equivalent pipe (i.e., a_e) can be solved from Eq. (9). The unknown variables in Eq. (10) are the transmission coefficients $T_s^{P_3 \to N_1}$ and $T_s^{P_e \to N_2}$, which are

all related the characteristic impedance of the equivalent pipe (i.e., $B_e = a_e/(gA_e)$). Therefore, the optimized B_e can be obtained by solving Eq. (10), then the diameter of the equivalent pipe (i.e., D_e) can be calculated from B_e and the previously obtained a_e in Eq. (9). Following the continuity of fluid transportation, the flow rate through the equivalent pipe can be calculated as $Q_e = Q_1 - rq_3 = Q_2 + (1-r)q_3$. As a result, the H-W coefficient (i.e., C_e) can be obtained from Eq. (11).

Consequently, the two-step transient-based skeletonization of series pipes with internal demands can be determined by solving Eq. (8) through Eq. (11) to obtain the demand allocation coefficient (i.e., r) and the attributes of the equivalent pipe (i.e., L_e, a_e, D_e and C_e). Particularly, the proposed method is also applicable to the case of pipes with no internal demand by setting $q_3 = 0$ (i.e., $Q_e = Q_1 = Q_2$). Moreover, the steady-state equivalence has been simultaneously implemented during this proposed skeletonization method through the uses of weighting factor r (for mass balance) in Step 1 and the C_e in Eq. (11) (for energy conservation) in Step 2. From this perspective, the proposed method is generic for the skeletonization of pipes in series accounting for transient dynamics.

Implementation of the generic transient-based skeletonization method

Within the proposed two-step skeletonization method, both the demand allocation and the series pipe merging would introduce skeletonization errors, which are represented by the indicators E_d and E_s in Eqs. (8) and (10) respectively. For practical applications, the indicator of the skeletonization errors by the proposed method can be specified to an acceptable range, that is

$$E = \max\left(E_d, E_s\right) \le E_{tol} \tag{12}$$

where E indicates the maximum error induced by skeletonization; E_{tol} is the specific maximum tolerable error specified by users. Referring to the definitions of E_d and E_s as the sum of weighted squared residuals in Eqs. (8) and (10), a smaller value of E_{tol} approaching to zero would result a more accurate skeletonized system. In other words, the accuracy of model skeletonization can be effectively controlled in advance based on the specific requirements of WDS modeling and analysis (i.e., the skeletonization level is determined by E_{tol}). As a result, E_{tol} is taken as the accuracy control metric for the transient-based skeletonization. It is noted the actual skeletonization error can be larger than the value of the E_{tol} indicator due to complicated transient mechanism including the superposition, diversion and dissipation of transient pressure waves at nodes and through pipelines. However, this indicator can be a meaningful surrogate to indirectly represent the underlying skeletonization errors that are very difficult to be characterized so far. Application procedures of the proposed method are shown in Fig. 3.

Investigating different demand allocations on transient dynamics

To investigate the impacts of different demand allocations on transient dynamics within the skeletonization of PSIDs, four skeletonization methods with different demand allocation strategies are implemented to enable a performance comparison. These are: (i) the proposed generic transient-based method (TBM) in this study; (ii) the steady-state based method with the internal demands equally allocated (SBM-EA); (iii) the steady-state based method with the internal demand proportionally allocated based on pipe lengths (SBM-PA); and (iv) the transient-based method with equal

329 demand allocation (TBM-EA). Among these methods, the SBM-EA and SBM-PA
330 have been typically used in the steady-state approaches without the consideration of
331 transient dynamics (e.g., Cesario 1995; Walski et al. 2003).

332 For the SBM-EA, the internal demand is equally allocated and the diameter of the
333 skeletonized pipe (D_e) is set to be the larger diameter of the two series pipes. This is
334 followed by that the length of the skeletonized pipe (L_e) is taken as the sum of series
335 pipes, with wave speed of the skeletonized pipe (a_e) determined following Eq. (9).
336 Finally, the H-W coefficient of the equivalent pipe (C_e) is determined based on Eq.
337 (10). The implementation of the SBM-PA is similar to the SBM-EA, except that the
338 internal demand is proportionally allocated based on pipe lengths in the SBM-PA. For
339 the TBM-EA, the internal demand is equally allocated to both end nodes (r = 0.5), and
340 the other implementation procedures are identical to the proposed TBM.

341 Extensive numerical experiments regarding different internal demand values and
342 different demand allocation strategies for the skeletonization of PSIDs are designed to
343 explore the impacts of demand allocation strategies on transient dynamics.
344 Specifically, a large number of different demand scenarios increased from small
345 values (e.g., 2 L/s) to large values (e.g., 20 L/s) are considered. For each demand
346 scenario, different demand allocation strategies with r ranging from 0 to 1 are used to
347 investigate the transient impacts induced by different demand allocation strategies,
348 conditioned on the fixed pipe attributes. Additionally, for a fixed r, a range of different
349 values of pipe attributes are used to investigate transient impacts induced by the
350 adjustments of pipe attributes within the skeletonization process.

Accuracy assessment metrics for the skeletonized systems

To assess the performance of the skeletonized systems produced by the different skeletonization methods, two accuracy assessment metrics are proposed in this paper. The first metric is the relative average difference in the transient pressure trajectories with time evolution for a node (i.e., err_{mean}), defined as

$$err_{mean} = \frac{\sum_{t=t_1}^{t_2} \left| H_0(t) - H_s(t) \right|}{N \cdot \Delta H_{fluc}} \times 100\% \tag{13}$$

where $H_0(t)$ and $H_s(t)$ are the transient pressure at any given simulation time t resulted from the original and skeletonized systems, respectively; t_1 and t_2 are the instants that the transient status starts to change and terminates to the final steady-state status, respectively, with N being the total number of instants between t_1 and t_2. $\Delta H_{fluc} = \max(H_0) - \min(H_0)$ represents the maximum pressure fluctuation during the transient process in the original system, therefore is used as the reference of the relative assessment metrics.

Additionally, it is generally more concerned about the performance of the skeletonized system in reproducing the extreme conditions, as such conditions often pose serious threats to the safety of WDSs. To address this concern, another metric to assess the relative difference in the extreme pressures during the transient process for a node (i.e., err_{ext}), is proposed as follows

$$err_{ext} = \frac{\Delta H_{ext}}{\Delta H_{fluc}} \times 100\% \tag{14}$$

where $\Delta H_{ext} = \max\left[\left|\max(H_0) - \max(H_s)\right|, \left|\min(H_0) - \min(H_s)\right|\right]$ is the absolute difference in the extreme transient pressures, which is taken as the greater value of the two following sources: (i) the difference of the maximum transient pressures between the original and skeletonized systems; and (ii) the difference of the minimum transient pressures between the two models.

Case studies

Description of two case studies

Two cases of a transmission pipeline system and a realistic WDS are used to demonstrate the feasibility of the proposed transient-based skeletonization method and investigate the impacts of nodal demand allocations on transient dynamics within the skeletonization process. Case 1 (Fig. 4a) is composed of two reservoirs, two control valves, pipes in series and nodes with demands. The series pipes [2], [3] and [4] are to be skeletonized with the internal demands at nodes 2 and 3 allocated to end nodes. Two different subcases are considered for Case 1, with identical and different characteristic impedances of the series pipes respectively (i.e., B_2, B_3 and B_4 for pipes [2], [3] and [4] as shown in Table 1). Other information for Case 1 is also listed in Table 1. Case 2 (Fig. 4b) is retrieved from a realistic benchmark WDS of the Modena network (MOD) (Bragalli et al. 2012), which consists of 4 reservoirs, 317 pipes and 268 nodes. 182 pipes in series can be identified to be skeletonized in this model. In Case 2, a typical wave speed of 1000 m/s for metal pipes is assigned for all pipes in the model.

Regarding the transient simulations for two cases, the classical one-dimensional water hammer model is adopted, with the method of characteristics (MOC) coupled with the

discrete vapor cavity model (DVCM) as transient solvers. The details of transient models and methods can be referred to many classic references (e.g., Chaudhry 2014; Zhu et al. 2018). The computational time steps for transient simulations of the two cases are set to be sufficiently small (i.e., 0.1 s for case 1 and 0.01 s for case 2). This is followed by the use of wave speed adjustments for pipe discretization, in order to satisfy the Courant condition with C_r = 1. In addition, the wave speed adjustments used in this study are trivial (no wave speed adjustment is used for case 1 and the average adjustment is less than 2.5% for case 2), and hence the resultant influence on transient analysis can be negligible.

Numerical Applications

Four skeletonization methods (i.e., TBM-Max, SBM-EA, SBM-PA and TBM-EA) are applied for both studied cases. It is noted that the proposed TBM using the maximum probability (TBM-Max) and that using the expectation in Fig. 2(b) exhibit similar performance, implying that the results are not significantly affected by the use of the maximum probability or expectation. For both subcases in Case 1, 10 transient events of different intensities (Table 2) are used to analyze the performances of the skeletonized systems produced by the four different methods. Different demand scenarios, with demands at nodes 2 and 3 identically ranging from 2 L/s to 10 L/s with an interval of 2 L/s, are considered for analysis. In addition, statistical analysis of the accuracy assessment metrics err_{mean} and err_{ext}, including the rankings of metric values from small to large and the distributions of cumulative probability function (CDF), are performed for different skeletonized systems resulted from different methods.

For this simple case, extensive simulation experiments are designed to explore the potential impacts of different demand allocation strategies on transient dynamics of the skeletonized system. For both subcases, 10 different demand scenarios are considered to investigate the impacts of different demand allocation strategies on transient dynamics, with demands at nodes 2 and 3 identically increasing from 2 L/s to 20 L/s with an interval of 2 L/s (Fig. 4a). Three experiments (i.e., E1, E2 and E3) are designed for each demand scenario, with details given in Table 3. For each experiment (E1, E2 and E3), all the transient events in Table 2 are applied to the original and skeletonized systems. Three assessment metrics including err_{mean}, err_{ext} and ΔH_{ext} (see Eqs. 13 and 14) are used to compute the skeletonization errors, and boxplots of the maximum and mean values of the resultant assessment metrics for all the simulations are used to enable the performance analysis.

For Case 2, different values of the tolerable error E_{tol} (e.g., 0.001, 0.01 and 1.00 respectively) are adopted for the proposed method to produce skeletonized systems with different skeletonization levels. To systematically compare the performances of these skeletonized systems, a total of 61 different transient events are produced by placing and operating the valve on each of 61 pipes that are not removed within the entire skeletonization process (i.e., each transient event is mimicked by fully closing a valve in 10 s with the initial velocity through the valve ranging from 0.01 m/s to 1.99 m/s among the 61 transient events). The statistical analysis of the accuracy assessment metric values, including the rankings and the CDFs for err_{mean} and err_{ext}, are also performed in this case.

Results and discussions

Results and analysis for Case 1

For the SBM-EA and TBM-EA applied to Case 1, $r_1 = r_2 = 0.5$ are consistently used. For SBM-PA, $r_1 = 0.58$, $r_2 = 0.80$ are used for Subcase 1 and $r_1 = 0.38$, $r_2 = 0.53$ are used for Subcase 2, which are determined based on the pipe length. In the proposed TBM-Max, these demand allocation coefficients are optimized by Eq. (8) for each demand scenario, with results presented in Table 4. By inspection, the optimal demand allocation coefficients of the proposed TBM-Max vary as a function of nodal demand values, which are all quite different with the pre-determined values of the traditional methods (e.g., $r_1 = r_2 = 0.5$).

Results of accuracy assessment metrics based on Eq. (13) and Eq. (14) are obtained for the four methods, with the rankings (i.e., the ranking values from 1 to 4 indicate the metric values from smallest to largest, which represents the accuracy decreasing in transient results) and CFDs of the metric values given in Figs. 5 and 6 respectively. Noting that the results of SBM-EA and TBM-EA are exactly identical for Subcase 1 since the pre-determined allocation coefficients (r) are the same for these two methods (i.e., demands are equally assigned to the end nodes) as well as that the diameters of series pipes (i.e., the characteristic impedances of series pipes) are identical. Fig. 5 and Fig. 6 clearly show that the proposed TBM-Max exhibit the overall best performances in reproducing the transient dynamics of the original full system. This is followed by TBM-EA, and then SBM-EA and finally SBM-PA. More specifically, as shown in Fig. 5(a) and Fig. 6(a), the probabilities of the first rankings are higher than 95% and 75% for the proposed TBM-Max applied to two subcases of Case 1 respectively, while these values are lower than 5% and 25% for the TBM-EA.

462 The superior performance of the proposed TBM-Max relative to the three traditional
463 skeletonization approaches can be also demonstrated by the error CDF profiles in Fig.
464 5(c, d) and Fig. 6(c, d).

465 Regarding the two transient-based methods (TBM-Max and TBM-EA), the proposed
466 TBM-Max are observed to exhibit better performance based on the results in Figs. 5
467 and 6. This is because that the TBM-Max considers the minimization of both
468 skeletonization errors induced by the allocation of internal demands and the merging
469 of series pipes with different attributes, while the TBM-EA only considers the latter.
470 This shows that different demand allocation strategies can significantly affect the
471 transient performance of the skeletonized system. Therefore, it is important and
472 necessary to account for the demand allocations within the skeletonization process.

473 Figures 7 and 8 show the statistical results of the maximum and mean errors of the
474 assessment metric values obtained from the simulation experiments given in Table 3.
475 Fig. 7(a-c) and Fig. 8(a-c) give the results of the experiment E1, Fig. 7(d-f) and Fig.
476 8(d-f) present results of E2, and Fig. 7(g-i) and Fig. 8(g-i) show results of E3. The
477 difference between the minimum and maximum values for each box in the figures
478 represents the variation range of the assessment metric due to different demand
479 allocation strategies or different characteristic impedances of the equivalent pipe.

480 It can be observed from Fig. 7(a-f) and Fig. 8(a-f) that, as nodal demands increase, the
481 variation ranges of the err_{mean}, err_{ext} and ΔH_{ext} due to different demand allocation
482 strategies generally increase in both experiments E1 and E2 where diameters of series
483 pipes are identical or different. For instance, the variation range of the maximum
484 ΔH_{ext} in Fig. 7(c) is only about 1.5 m for the nodal demand of 2 L/s, but it increases

485 up to about 8.7 m for 12 L/s. This indicates that the extent of the transient impacts
486 induced by demand allocation strategies varies as a function of demand values, with
487 larger nodal demand values showing larger influence. Results also suggest that the
488 demand allocation during the skeletonization process can be significant in affecting
489 transient dynamics especially when the demand values are moderate-large (Huang et
490 al. 2017).

491 Fig. 7(d-i) and Fig. 8 (d-i) demonstrate the relative importance between the transient
492 impacts induced by different demand allocations and that caused by the variation of
493 pipe characteristic impedances for different demand scenarios. As shown in these
494 figures, when the nodal demands are relatively small (e.g., 2 L/s), the variation of
495 three assessment metric values (err_{mean}, err_{ext} and ΔH_{ext}) caused by different demand
496 allocations are overall limited. However, if the internal demands are moderate or
497 reasonably large, the extent of the transient impacts induced by the demand
498 allocations can be comparable to or even greater than those caused by the variation of
499 pipe characteristic impedances. For example, for the demand scenario with 10 L/s, the
500 variation range of err_{ext} and ΔH_{ext} induced by different demand allocation strategies
501 in Fig. 8(e, f) are 8.3% and 2.2 m, which are similar to those caused by pipe attributes
502 (Fig. 8(h, i)). When the internal demands of nodes 2 and 3 increase to a large value
503 with 16 L/s, the variation ranges of the three assessment metric values in Fig. 8(d, e, f)
504 are greater than those in Fig. 8(g, h, i). These findings indicate that both the strategies
505 of the internal demand allocation and the merging of series pipes with different
506 attributes should be thoroughly considered during the transient-based skeletonization
507 process of WDSs, especially when the demand values are moderate-large.

Results and analysis for Case 2

For Case 2, three different values of the tolerable error E_{tol} (i.e., 0.001, 0.01 and 1.00) are tested to regulate the skeletonization process using the proposed TBM-Max, with the resultant skeletonized systems shown in Fig. 9. To enable a fair comparison, skeletonized systems are also produced using the other three methods (SBM-EA, SBM-PA and TBM-EA). Fig. 9 shows that a larger value of E_{tol} would produce a skeletonized system with a higher skeletonization level (i.e., Level 1, Level 2 and Level 3 corresponding to E_{tol} = 0.001, 0.01 and 1.00 respectively), where the skeletonization level refers to the number proportion of nodes that has been removed within the original model by the skeletonization process. Note that the series pipes skeletonized within Level 1 are assigned with identical characteristic impedances, and hence the skeletonization error is mainly induced by demand allocations. For Levels 2 and 3, both the demand allocation and series pipes merging strategies are involved in the skeletonization process. Particularly, 182 out of the 317 pipes in this studied system have been skeletonized within Level 3.

Fig. 10 shows the overall distribution of the demand allocation coefficients (i.e., 182 optimized r values) for the skeletonization using TBM-Max with E_{tol} =1.0 (Level 3). The resultant demand allocation coefficients exhibited a nonuniform distribution in the entire variation domain (i.e., 0~1), which is significantly different from the commonly-used equal demand allocation in traditional approaches (i.e., r = 0.5). This finding, together with that obtained in Case 1 (Table 4), demonstrates again that different demand allocation strategies can significantly affect the transent dynamics of the WDSs within the skeletonization proces, and r = 0.5 is not necessary the optimal allocation strategy.

As indicated previously, 61 transient events have been planned and applied for Case 2 to enable an overall performance comparison between the skeletonized systems resulted from different methods. The ranking and CDF results of the two proposed assessment metrics for different skeletonization methods and different levels of the skeletonized systems are presented in Figures 11 and 12, respectively. From these results, it can be seen that TBM-Max consistently exhibits the best performance, followed by TBM-EA, SBM-EA and SBM-PA. For example, as shown in Fig. 11(a, c, e), the probabilities of the first rankings based on the err_{mean} for the three skeletonization levels are about 80%, 60% and 55% respectively for the proposed TBM-Max. These values are consistently significantly higher than those for the TBM-EA, SBM-EA and SBM-PA. Similar findings can be also observed in Fig. 12 as the CDF profiles of TBM-Max are higher than those of the other three traditional methods. Fig. 11 also shows that the probabilities of the first rankings for the TBM-Max increase when the skeletonization level decrease (e.g., from Level 3 to Level 1). This implies that the superiority of the TBM-Max become more prominent when demand allocations are only involved within the skeletonization process, which is often the case when the series pipes have identical attributes (e.g., diameters).

Investigation of transient pressure traces in different skeletonized systems

Transient results of pressure traces at nodes from the original systems and different skeletonized systems produced by different methods are taken from the two studied cases for further investigation, with results shown in Fig. 13. The proposed method (TBM-Max) and one of the traditional methods (i.e., SBM-EA) are selected for comparison. Figs. 13(a) and (b) present the results of transient pressure traces with occurrences of vapor capacities to investigate the performances of the skeletonized

556 systems in modeling extreme transient events that are generally concerned by
557 modelers and practitioners (e.g., cavitation phenomenon). More specifically, Fig. 13(a)
558 indicates the transient results at the downstream of valve 1 in the subcase 1 of case 1
559 (Fig. 4a) for the skeletonized systems resulted from the demand scenarios of 10 L/s.
560 Fig. 13(b) presents the transient results of Node 1 in case 2 (Fig. 4b) for the
561 skeletonized systems of Level 3. In addition, Figs. 13(c) and (d) show the transient
562 results at the same node selected in case 2 (i.e., Node 2 in Fig. 4b) from the
563 skeletonized systems of Levels 1 and 3 respectively, to demonstrate the different
564 transient responses in skeletonized systems with different skeletonization levels.

565 As shown in Fig. 13, it can be generally observed that the proposed TBM-Max
566 exhibits a better performance than the traditional SBM-EA in capturing the overall
567 transient dynamics of the original system. Specifically, 13(a) and (b) shows that the
568 TBM-Max significantly outperforms the SBM-EA in terms of both the transient
569 amplitudes and phases, especially in modeling the formation and collapse of cavities.
570 Nevertheless, it should be acknowledged that the proposed transient-based method
571 still cannot accurately capture the entire transient dynamics during the transient
572 evolution (e.g., the timing and amplitude of the cavity collapse), which should be
573 aware by practitioners. The comparison between Figs. 13(c) and (d) indicates that the
574 superiority of the TBM-Max becomes more prominent for a higher skeletonization
575 level where the allocations of moderate-large demands (e.g., 4~10 L/s as investigated
576 in case 1) and the merging of series pipes with different attributes are both involved.
577 However, for the case that the skeletonization only involves the allocations of
578 relatively small demands (e.g., Fig. 13c), the skeletonized systems from the proposed
579 and traditional methods can overall match the original system in transient dynamics.
580 Similar observations can be made for transient traces at other nodes as well as other

581 transient events for both cases.

582 ## Summary and conclusions

583 This paper proposes a generic transient-based method with transient dynamics
584 explicitly considered to skeletonize pipes in series with internal demands and makes
585 the first attempt to investigate the impacts of nodal demand allocations on transient
586 dynamics within the skeletonization process. A two-step skeletonization procedure has
587 been proposed in this study – the internal nodal demand allocation and the series pipes
588 merging. Two optimization approaches are accordingly developed to minimize the
589 skeletonization errors induced by the two operations with coupling the accuracy
590 control criteria for both steady-state and transient responses in WDS (i.e., the phase
591 criterion and the amplitude criterion). A probabilistic approach based on Monte-Carlo
592 simulations (MCS) for evaluating the nodal demand effect on transient dynamics is
593 also incorporated within the procedure for the internal demand allocation. Two
594 accuracy assessment metrics are defined to quantitatively evaluate the performance of
595 the skeletonized systems.

596 The utility of the proposed method is demonstrated using two cases studies, where
597 one case is a transmission pipeline system and the other case is a realistic benchmark
598 WDS. Meanwhile, the transient impacts induced by nodal demand allocation
599 strategies are investigated for different demand scenarios (i.e., 2~20 L/s in the studied
600 cases). The application and investigation results generally indicate that the extent of
601 the impacts of nodal demand allocations on transient dynamics is positively correlated
602 with the nodal demands. In addition, the proposed transient-based method (TBM)
603 outperforms the traditional steady-state based methods (SBM-EA and SBM-PA) in

604 capturing the transient dynamics of the original systems with different degrees under
605 different demand conditions. More specifically, when the nodal demands are
606 relatively small (e.g., below 2 L/s for the studied cases), the transient impacts of nodal
607 demand allocations are trivial and the proposed method only outperforms the
608 traditional methods marginally. This implies that the traditional methods are usually
609 sufficient in accurately capturing the transient dynamics of the original systems in
610 such cases. However, when the nodal demands are moderate-large (e.g., greater than 2
611 L/s), the transient impacts of nodal demand allocations can be relatively large (these
612 impacts can be comparable to or even greater than those caused by the merging of
613 series pipes with different attributes), and in such cases the advantage of the proposed
614 method becomes more significant than the traditional approaches. Therefore, the
615 proposed method is practically meaningful as it can identify skeletonized systems that
616 have better ability to represent the transient dynamics of the original WDS than the
617 traditional methods, especially for WDS nodes with relatively large demands.

618 To generalize the finding of the current study for practical implementations, a metric
619 that represents the ratio of the nodal demands relative to the pipe flows through this
620 node can be considered. In addition, the initial velocity of the pipe flows should be
621 also accounted for within the skeletonization process. This is because the impact
622 extent of nodal demand allocations on transient dynamics can be also affected by
623 other factors, such as the pipe flows through the demand nodes, the initial velocity
624 and the variation of the nodal demands during the operation of the system. Therefore,
625 an important future study should be undertaken to further explore these factors,
626 thereby offering an important and simple guideline for practical applications. It is also
627 noted that the users with large demands and nodes with relatively high elevations
628 should be carefully treated during the skeletonization process and in many cases such

629 nodes are not eliminated from the system.

630 It is acknowledged that there exist a few limitations of the current study that need to
631 be addressed in future studies. The first and important limitation is that the relative
632 computational efficiency between the original and skeletonized systems has not been
633 examined as the focus of the current study is to improve the transient precision within
634 the skeletonization process. While the skeletonized systems can allow a larger time
635 step for simulation, the increased time step can induce many discretization errors in
636 addition to those caused by wave speed changes and boundary approximations.
637 Therefore, it is very important to comprehensively investigate this issue in future as
638 the computational benefit associated with the skeletonized systems is practically
639 meaningful. The second limitation of this paper is that the skeletonized system may
640 vary as a function of changing demand distributions of the WDS over different time
641 periods, leading to a challenge for the practical implementation of the proposed
642 skeletonization method. An ad-hoc way to address this problem is to identify the
643 skeletonized system of the original WDS using nodal demands at the high demand
644 period. This is because transient dynamics at the high demand period (pipe velocities
645 are overall high during the high demand period) are often larger than those during the
646 low demand period. The third limitation is that many transient events considered in
647 this study have limited impacts to the system. Therefore, to further generalize the
648 findings of this study, transient events that can have a global impact on the system
649 should be considered in future. Finally, it is noted that the proposed approach should
650 be considered as a stage within the WDS analysis (rather than an end point) as the
651 selection of the skeletonization techniques may depend on the purpose of the WDS
652 models.

Acknowledgments

The corresponding author Professor Feifei Zheng was funded by The National Science and Technology Major Project for Water Pollution Control and Treatment (2017ZX07201004), Excellent Youth Natural Science Foundation of Zhejiang Province (LR19E080003) and The National Natural Science Foundation of China (grant number 51708491). Dr Duan was supported by the Hong Kong Research Grants Council (RGC) under project no. 15201017.

Data availability statement

Details of models, data or results used/generated during this study are available from the corresponding author by request.

References

AWWA. 2019. “Committee Report: Getting Started in Transient Analysis.” J. Am. Water Works Assoc. 111: 32-37. doi:10.1002/awwa.1269.

Boulos, P. F., B. W. Karney, D. J. Wood, and S. Lingireddy. 2005. “Hydraulic transient guidelines for protecting water distribution systems.” *J. Am. Water Works Assoc.* 97 (5): 111–124. https://doi.org/10.1002/j.1551-8833.2005.tb10892.x.

Bragalli C., D’Ambrosio C., Lee J., Lodi A., and P. Toth. 2012, “On the optimal design of water distribution networks: A practical MINLP approach,” *Optim. Eng.*, 13(2), 219–246.

Cesario, L. 1995. *Modeling, Analysis, and Design of Water Distribution Systems*. Ed. AWWA. Denver, USA.

675 Chaudhry, M. H. 2014. *Applied hydraulic transients*. New York: Springer.
676 Davis, M. J., and R. Janke. 2015. "Influence of network model detail on estimated
677 health effects of drinking water contamination events." *J. Water Resour. Plann.*
678 *Manage*. 141 (1): 04014044.
679 https://doi.org/10.1061/(ASCE)WR.1943-5452.0000436.
680 Davis, M. J., and R. Janke. 2018. "The effect of a loss of model structural detail due
681 to network skeletonization on contamination warning system design: case
682 studies." *Drinking water engineering and science*, 11(1), 49-65.
683 Deuerlein, J. W. 2008. "Decomposition model of a general water supply network
684 graph." *J. Hydraul. Eng.* 134 (6): 822–832.
685 https://doi.org/10.1061/(ASCE)0733-9429(2008)134:6(822).
686 Duan, H. F., Y. K. Tung, and M. S. Ghidaoui. 2010. "Probabilistic analysis of
687 transient design for water supply systems." *J. Water Resour. Plann. Manage.*
688 136(6), 678–687.10.1061/(ASCE)WR.1943-5452.0000074
689 Duan, H. F., and P. J. Lee. 2015. "Transient-based frequency domain method for
690 dead-end side branch detection in reservoir pipeline-valve systems." *J. Hydraul.*
691 *Eng.* 142 (2): 04015042. https://doi.org/10.1061/(ASCE)HY.1943-7900.0001070.
692 Ebacher, G., M. C. Besner, J. Lavoie, B. S. Jung, B. W. Karney, and M. Prévost. 2011.
693 "Transient modeling of a full-scale distribution system: Comparison with field
694 data." *J. Water Resour. Plann. Manage.* 137 (2): 173–182.
695 https://doi.org/10.1061/(ASCE)WR.1943-5452.0000109.
696 Gad, A. A. M., and H. I. Mohammed. 2014. "Impact of pipes networks simplification
697 on water hammer phenomenon." Sadhana. 39 (5): 1227–1244.
698 https://doi.org/10.1007/s12046-014-0260-7.
699 Gong, J., M. F. Lambert, A. R. Simpson, and A. C. Zecchin. 2014. "Detection of

700 localized deterioration distributed along single pipelines by reconstructive MOC
701 analysis." *J. Hydraul. Eng.* 140 (2): 190–198.
702 https://doi.org/10.1061/(ASCE)HY.1943-7900.0000806.
703 Gong, J., M. F. Lambert, S. T. N. Nguyen, A. C. Zecchin, and A. R. Simpson. 2018.
704 "Detecting thinner-walled pipe sections using a spark transient pressure wave
705 generator." *J. Hydraul. Eng.* 144 (2): 06017027.
706 https://doi.org/10.1061/(ASCE)HY.1943-7900.0001409.
707 Grayman, W. M., R. M. Males, and R. M. Clark. 1991. "The effects of skeletonization
708 on distribution system modeling." In *Proc., AWWA Seminar on Computers in the*
709 *Water Industry*, 661–684. Denver: American Water Works Association.
710 Hellbach, C., M. Möderl, R. Sitzenfrei, and W. Rauch. 2011. "Influence of network
711 properties and model purpose on the level of skeletonization." In *Proc., World*
712 *Environmental and Water Resources Congress 2011: Bearing Knowledge for*
713 *Sustainability*. 137–145. Reston, VA: ASCE.
714 Huang, Y., H.-F. Duan, M. Zhao, Q. Zhang, H. Zhao, and K. Zhang. 2017.
715 "Probabilistic analysis and evaluation of nodal demand effect on transient
716 analysis in urban water distribution systems." *J. Water Resour. Plann. Manage.*
717 143 (8): 04017041. https://doi.org/10.1061/(ASCE)WR.1943-5452.0000797.
718 Huang, Y., F. Zheng, H. F. Duan, T. Zhang, X. Guo, and Q. Zhang. 2019.
719 "Skeletonizing Pipes in Series within Urban Water Distribution Systems Using a
720 Transient-Based Method." *J. Hydraul. Eng*. 145(2), 04018084.
721 Jung, B. S., P. F. Boulos, and D. J. Wood. 2007. "Pitfalls of water distribution model
722 skeletonization for surge analysis." *J. Am. Water Works Assoc*. 99 (12): 87–98.
723 https://doi.org/10.1002/j.1551-8833.2007.tb08109.x.
724 Kapelan, Z. S., D. A. Savic, and G. A. Walters. 2007. "Calibration of water

distribution hydraulic models using a Bayesian-type procedure." *J. Hydraul. Eng*. 133 (8): 927–936. https://doi.org/10.1061/(ASCE)0733-9429(2007)133:8(927).

Martínez-Solano, F. J., P. L. Iglesias-Rey, D. Mora-Meliá, and V. S. Fuertes-Miquel. 2017. "Exact skeletonization method in water distribution systems for hydraulic and quality models." *Procedia Eng.* 186: 286–293. https://doi.org/10.1016/j.proeng.2017.03.246.

Martin, C. S. 2000. *Hydraulic transient design for pipeline systems.* New York: McGraw-Hill.

McInnis, D., and B. W. Karney. 1995. "Transients in distribution networks: Field tests and demand models." *J. Hydraul. Eng.* 10.1061/(ASCE)0733-9429(1995)121:3(218), 218–231.

Meniconi, S., B. Brunone, M. Ferrante, C. Capponi, C. A. Carrettini, C. Chiesa, D. Segalini, and E. A. Lanfranchi. 2015. "Anomaly pre-localization in distribution-transmission mains. Preliminary field tests in the Milan pipe system." *J. of Hydroinformatics, IWA.* 17(3), 377-389.

Meniconi, S., B. Brunone, and M. Frisinghelli. 2018. "On the role of minor branches, energy dissipation, and small defects in the transient response of transmission mains." *Water*. 10(2), 187.

Perelman, L., and A. Ostfeld. 2011. "Topological clustering for water distribution systems analysis." *Environ. Modell. Software.* 26 (7): 969–972. https://doi.org/10.1016/j.envsoft.2011.01.006.

Rathnayaka, S., R. Keller, J. Kodikara, and L. Chik. 2016. "Numerical simulation of pressure transients in water supply networks as applicable to critical water pipe asset management." *J. Water Resour. Plann. Manage.* 142 (6): 04016006. https://doi.org/10.1061/(ASCE)WR.1943-5452.0000636.

Saldarriaga, J. G., S. Ochoa, D. Rodriguez, and J. Arbeláez. 2008. “Water distribution network skeletonization using the resilience concept.” In *Proc., Water Distribution Systems Analysis 2008*. Reston, VA: ASCE.

Walski, T. M.. 1984. *Analysis of water distribution systems*. New York: Van Nostrand Reinhold Co..

Walski, T. M., D. V. Chase, D. A. Savic, W. M. Grayman, S. Beckwith, and E. Koelle. 2003. *Advanced water distribution modeling and management*. Waterbury, CT: Haestead Press.

Walski, T. M., J.-L. Daviau, and S. Coran. 2004. “Effect of skeletonization on transient analysis results.” In *Proc., ASCE EWRI Conf.* Reston, VA: ASCE.

Wood, D. J., S. Lingireddy, P. F. Boulos, B. W. Karney, and D. L. McPherson. 2005. “Numerical methods for modeling transient flow in distribution systems.” *J. Am. Water Works Assoc*. 97 (7): 104–115. https://doi.org/10.1002/j.1551-8833.2005.tb10936.x.

Wylie, E. B., V. L. Streeter, and L. Suo. 1993. *Fluid transients in systems.* Englewood Cliffs, NJ: Prentice Hall.

Zhang, Q., F. Zheng, H. F. Duan, Y. Jia, T. Zhang, and X. Guo. 2018. “Efficient Numerical Approach for Simultaneous Calibration of Pipe Roughness Coefficients and Nodal Demands for Water Distribution Systems.” *J. Water Resour. Plann. Manage.* 144(10): 04018063.

Zheng, F., Zecchin, A., Maier, H., and Simpson, A. (2016). "Comparison of the Searching Behavior of NSGA-II, SAMODE, and Borg MOEAs Applied to Water Distribution System Design Problems." *Journal of Water Resources Planning and Management*, 142(7), 04016017.

Zheng, F., Zecchin, A., Newman, J., Maier, H., and Dandy, G. (2017). "An Adaptive

775 Convergence-Trajectory Controlled Ant Colony Optimization Algorithm with
776 Application to Water Distribution System Design Problems." *IEEE Transactions*
777 *on Evolutionary Computation*, 21(5), 773-791.
778 Zhu, Y., Duan, H. F., Li, F., Wu, C. G., Yuan, Y. X., and Shi, Z. F. 2018.
779 "Experimental and numerical study on transient air-water mixing flows in
780 viscoelastic pipes." *Journal of Hydraulic Research* – IAHR, 56(6): 877-887.
781

782 **Table 1 Pipe information for Case 1**

Pipe	H-W coefficient	Wave speed (m/s)	Subcase 1			Subcase 2		
			Length (m)	Diameter (mm)	Impedance (s/m^2)	Length (m)	Diameter (mm)	Impedance (s/m^2)
[1]	115	1000	900	300	1442.1	900	300	1442.1
[2]	123	1000	700	**250**	**2076.6**	300	**300**	**1442.1**
[3]	113	1000	500	**250**	**2076.6**	500	**250**	**2076.6**
[4]	110	1000	300	**250**	**2076.6**	700	**200**	**3244.7**
[5]	117	1000	1000	200	3244.7	1000	200	3244.7

Note: the column “Impedance” indicates the characteristic impedances of pipes.

783

784

785 **Table 2 Planned transient events for Case 1**

Transient event	Transient exciter	Event description
1	Valve 1	Close 80% in 5 s and then close the other 20% in 15 s
2	Valve 1	Close 80% in 5 s and then close the other 20% in 30 s
3	Valve 2	Fully close in 15 s
4	Valve 2	Fully close in 30 s
5	Valve 2	Close 80% in 5 s and then close the other 20% in 15 s
6	Valve 2	Close 80% in 5 s and then close the other 20% in 30 s
7	Valve 1	Close 90% in 5 s and then fully open in 5 s
8	Valve 1	Close 90% in 30 s and then fully open in 5 s
9	Valve 2	Close 90% in 5 s and then fully open in 5 s
10	Valve 2	Close 90% in 30 s and then fully open in 5 s

786

787

788 **Table 3 Experiment design for Case 1**

Experiment index	Details of the experiment design	Objectives of the experiment
E1	For each demand scenario in Subcase 1, B_e = 2076.6 s/m^2 (determined by Eq. 9), r ranges from 0 to 1 with an interval of 0.1 for nodes 2 and 3.	To investigate the transient impacts induced by different demand allocation strategies when the values of B for series pipes are identical.
E2	For each demand scenario in Subcase 2, B_e = 2645.4 s/m^2 (determined by Eq. 9), r ranges from 0 to 1 with an interval of 0.1 for nodes 2 and 3.	To investigate the transient impacts induced by different demand allocation strategies when the values of B for series pipes are different.
E3	For each demand scenario in Subcase 2, r = 0.5 for nodes 2 and 3, B_e ranges from 3244.7 to 1442.1 s/m^2, corresponding to D_e ranging from 200 to 300 mm with an internal of 10 mm.	To investigate the transient impacts induced by the adjustments of pipe attributes, as well as to explore the relative importance of the transient impacts induced by demand allocations and pipe attributes.

789

790

791 **Table 4 Optimized demand allocation coefficients (*r*) of the proposed TBM-Max**
792 **for different demand scenarios of the two subcases of Case 1**

Demands at Nodes 2 and 3 (L/s)	Subcase 1		Subcase 2	
	r_1	r_2	r_1	r_2
2	0.47	0.18	0.78	0.69
4	0.46	0.18	0.78	0.71
6	0.44	0.17	0.78	0.72
8	0.42	0.16	0.77	0.72
10	0.40	0.15	0.76	0.73

Note: r_1 and r_2 represent the two optimized demand allocation coefficients in sequence for the skeletonization of series pipes [2], [3] and [4].

793

794

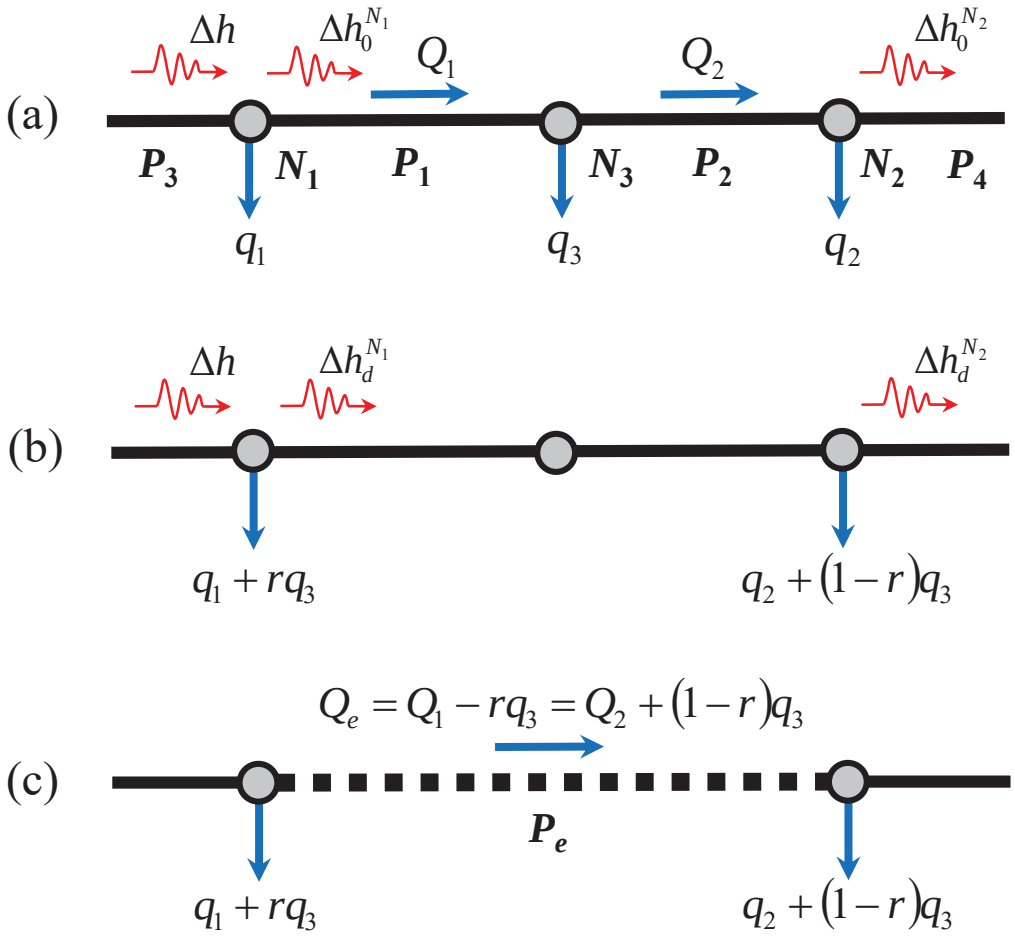

Fig.2

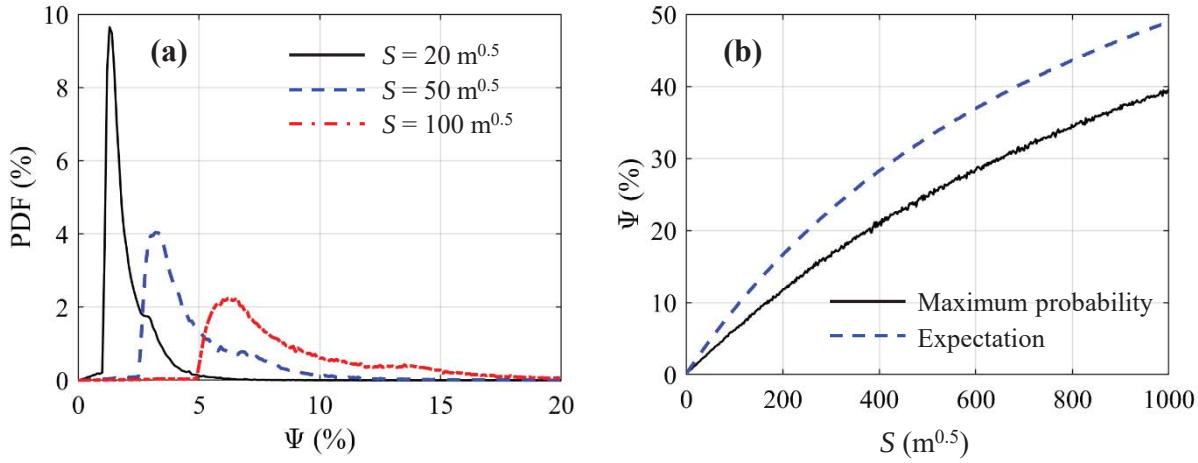

Fig.3

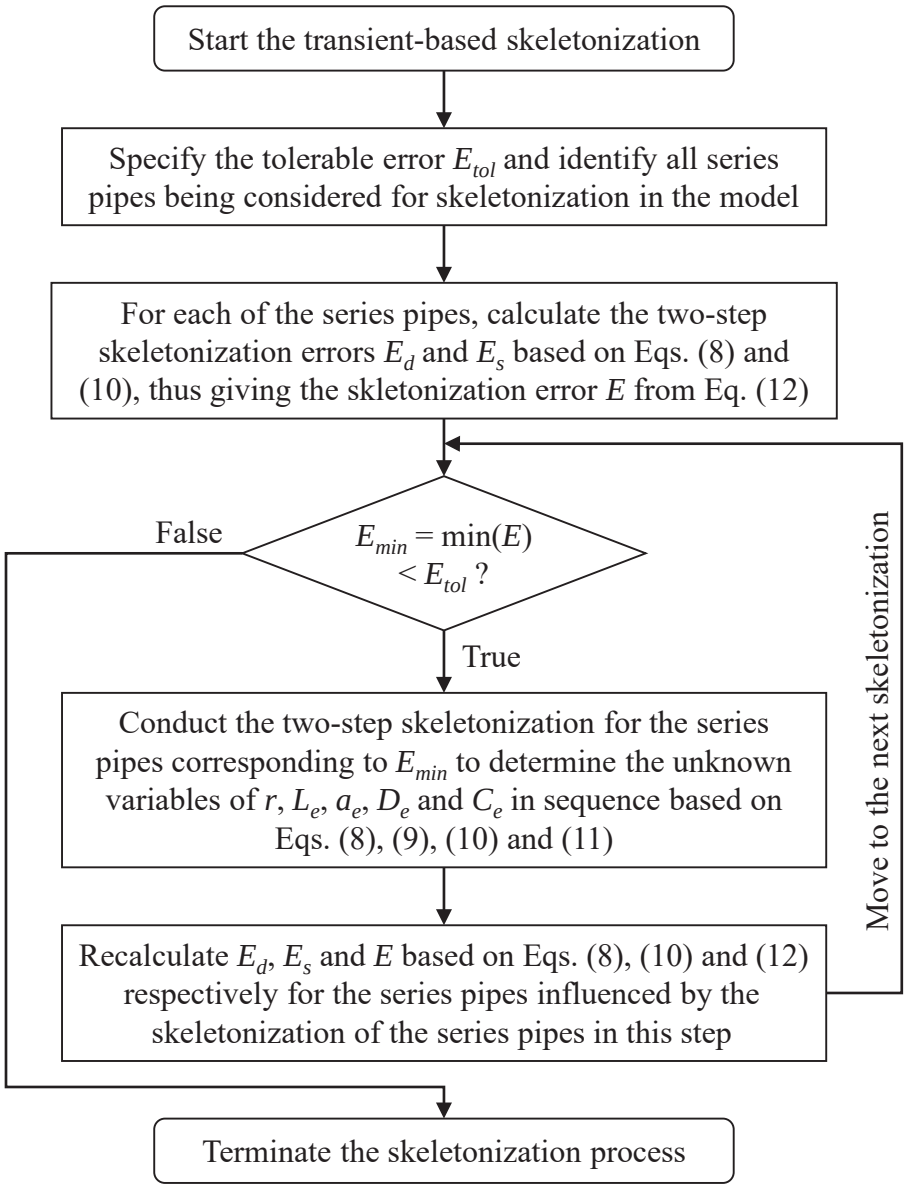

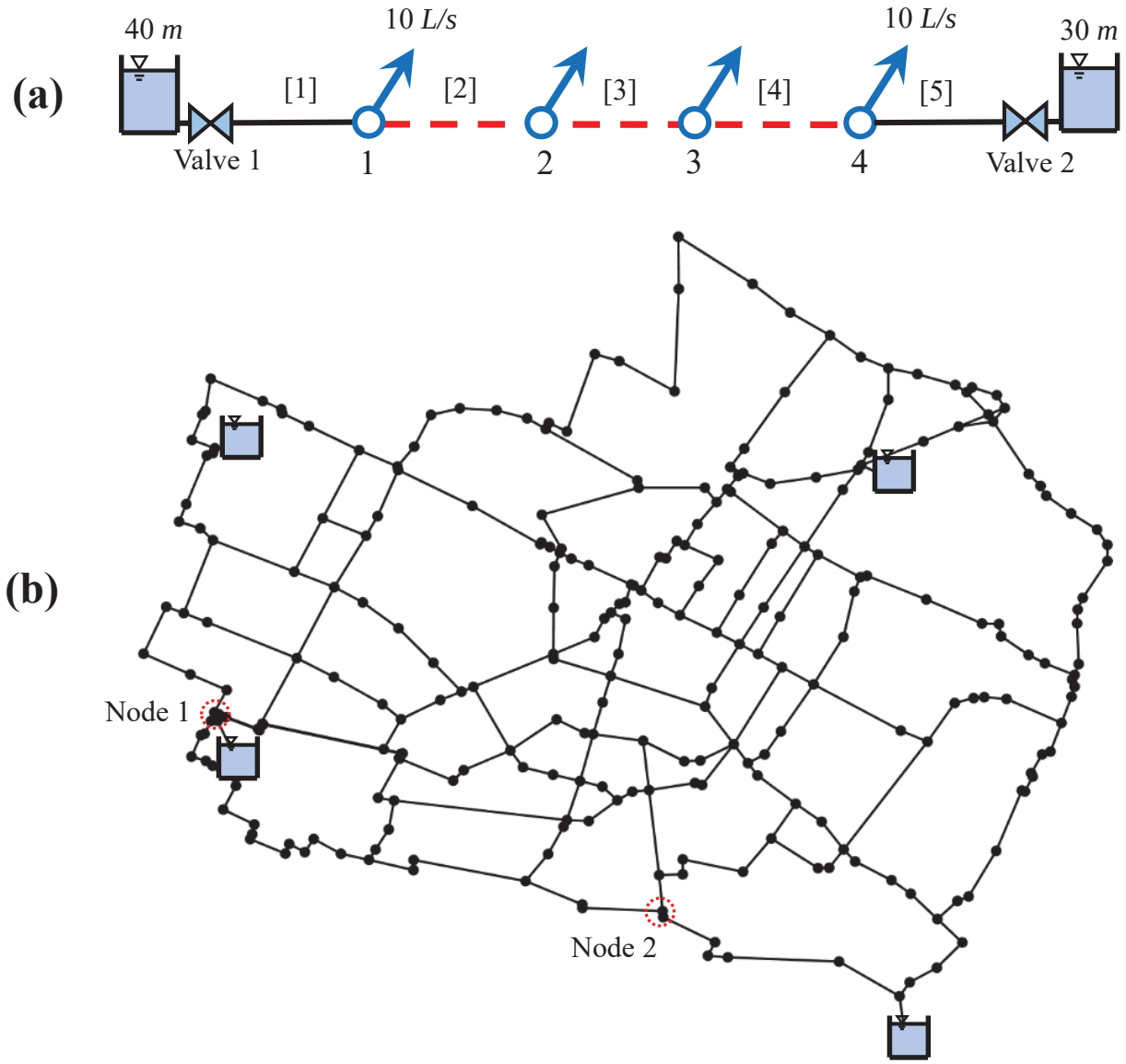

Fig.5

Click here to access/download;Figure;Fig.5.pdf

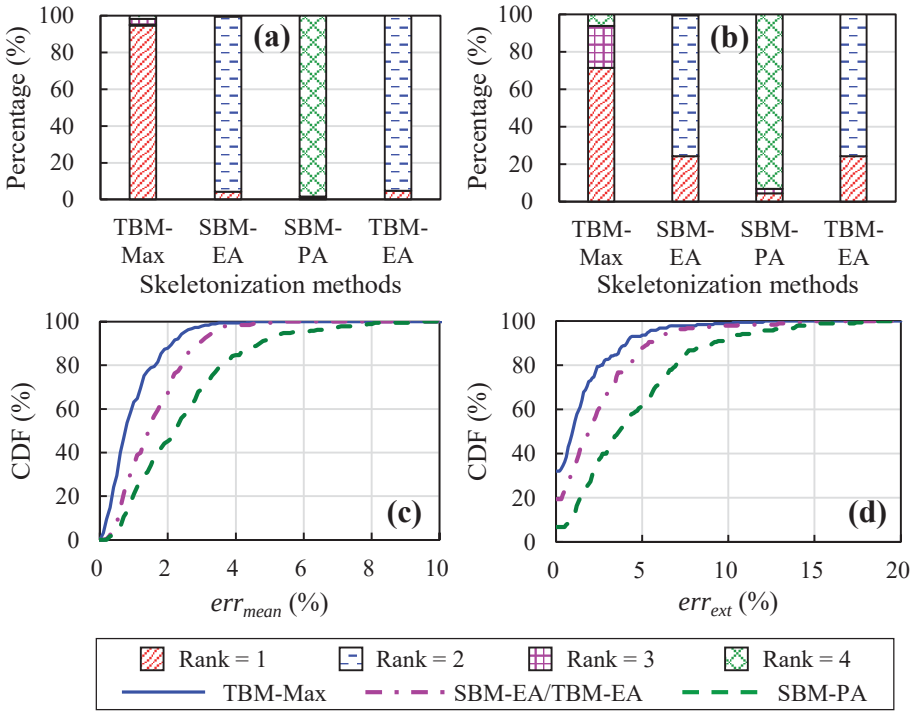

Fig.6

Click here to access/download;Figure;Fig.6.pdf

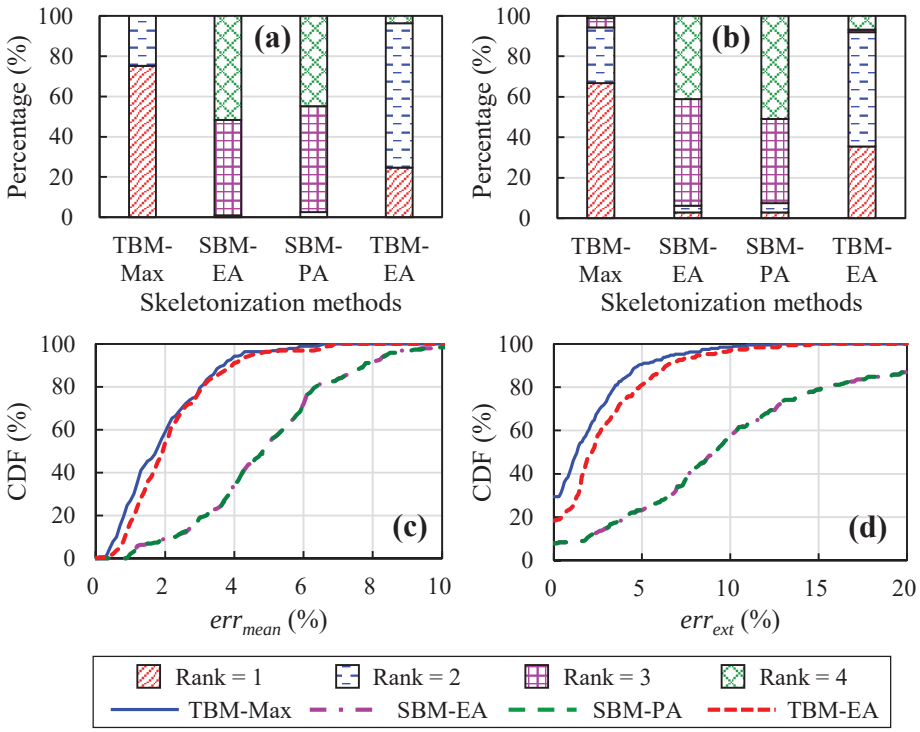

Fig.7

Click here to access/download;Figure;Fig.7.pdf

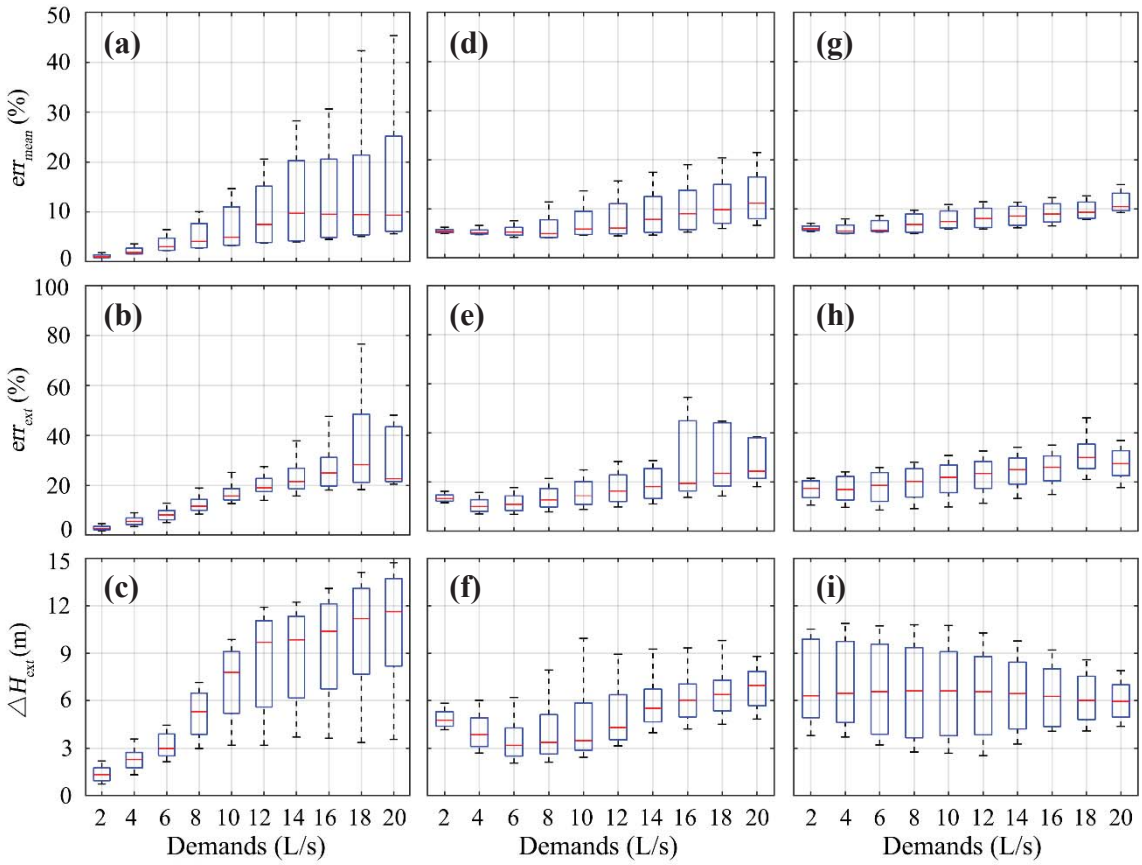

Fig.8

Click here to access/download;Figure;Fig.8.pdf

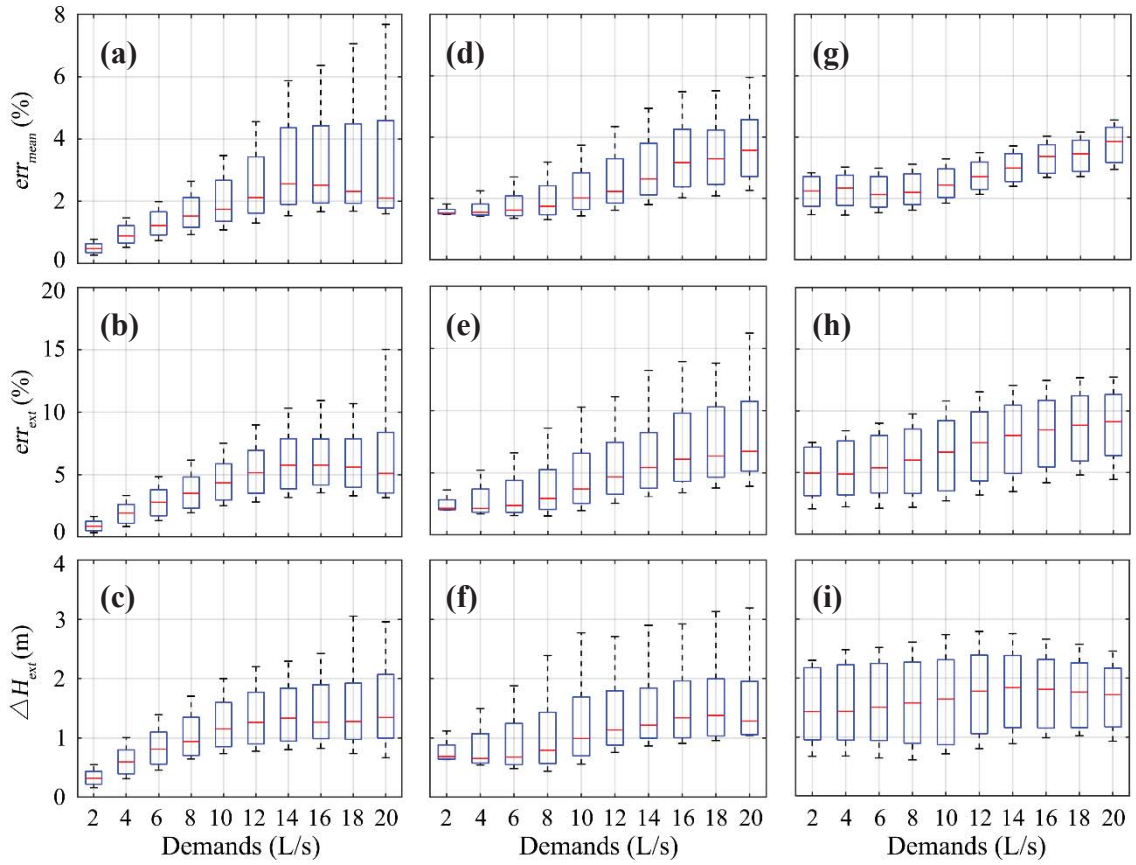

Fig.9

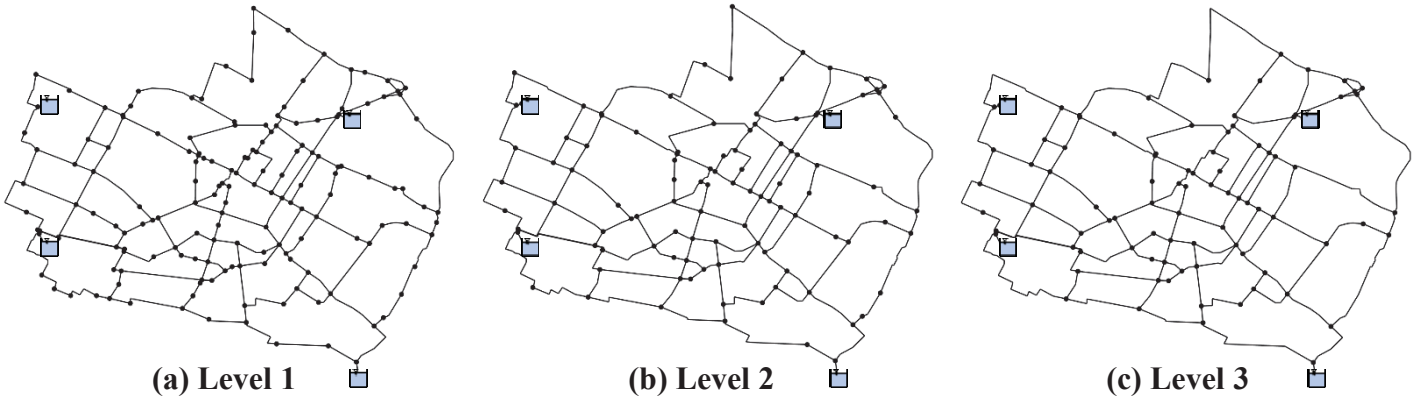

(a) Level 1 (b) Level 2 (c) Level 3

Fig.10

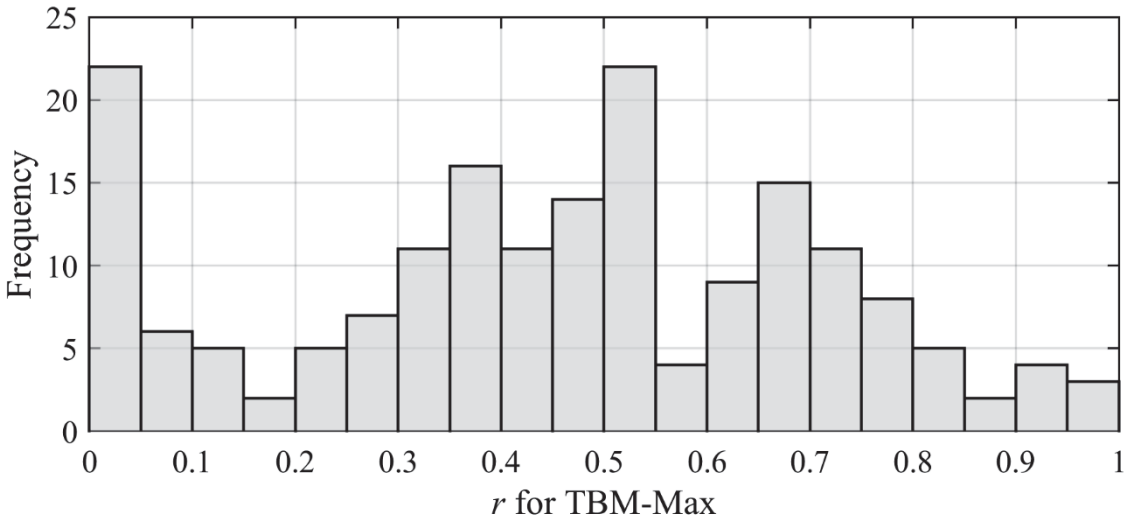

Fig.11

Click here to access/download;Figure;Fig.11.pdf

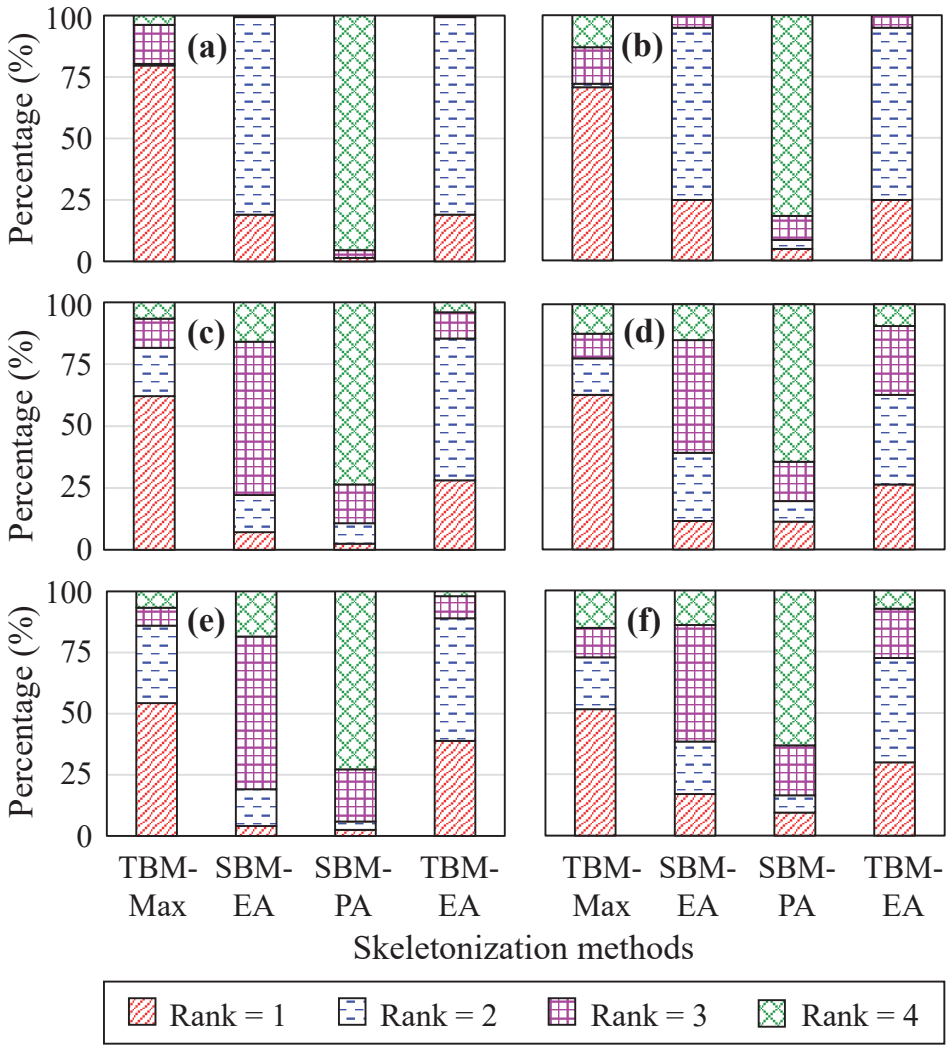

Fig.12

Click here to access/download;Figure;Fig.12.pdf

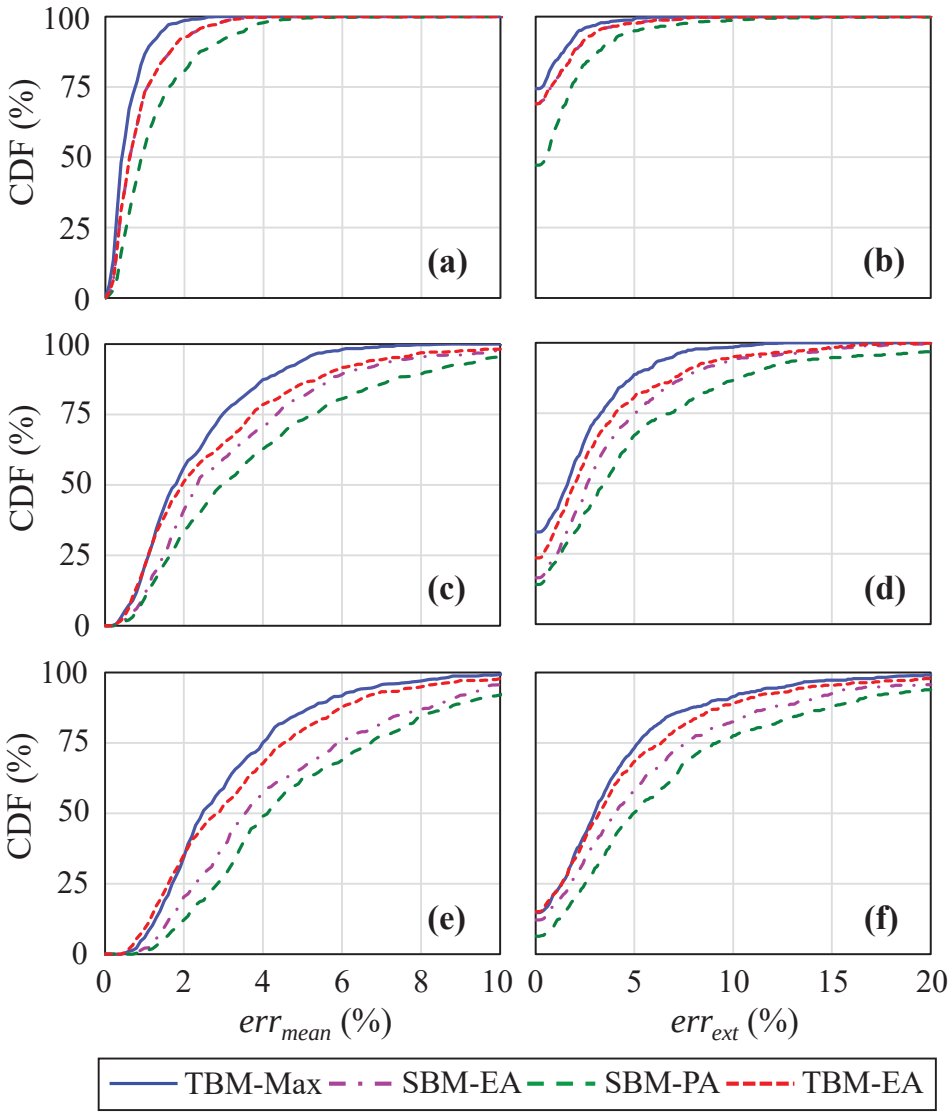

Fig.13

Click here to access/download;Figure;Fig.13.pdf

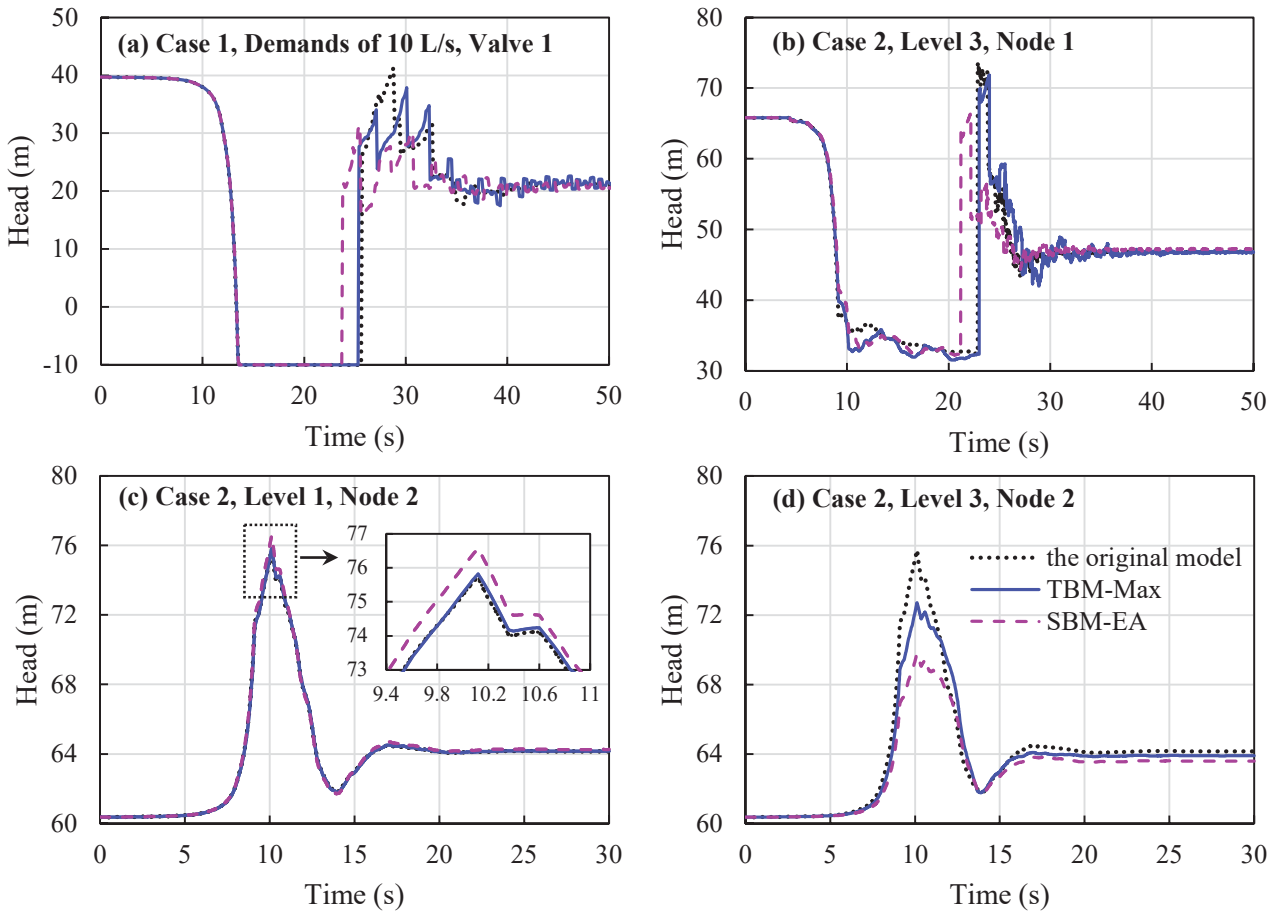

Fig. 1 Illustrative example of series pipes with internal demands for the two-step skeletonization: (a) the original system; (b) Step 1: the internal demand allocation; and (c) Step 2: merging pipes in series

Fig. 2 Probabilistic evaluation of nodal demand effect: (a) probability density functions (PDFs) for different static attributes (S = 20, 50 and 100 $m^{0.5}$); (b) statistical parameter mapping of maximum probability and expectation for nodal demand effect (Ψ) with respect to the static attributes (S)

Fig. 3 Flowchart for the implementation procedure of transient-based skeletonization method in WDS models

Fig. 4 Network layouts of two studied cases: (a) a simple transmission pipeline system; (b) the realistic network in MOD

Fig. 5 Ranking and CDF results of different skeletonization methods for subcase 1 with (a, c) for err_{mean} and (b, d) for err_{ext}

Fig. 6 Ranking and CDF results of different skeletonization methods for subcase 2 with (a, c) for err_{mean} and (b, d) for err_{ext}

Fig. 7 Boxplots of the maxium errors of the assessment metric values for different demand scenarios. Results of (a-c), (d-f) and (g-i) refers to E1, E2 and E3 in Table 3 respecitively. Red line is the median value.

Fig. 8 Boxplots of the mean errors of assessment metric values for different demand scenarios. Results of (a-c), (d-f) and (g-i) refers to E1, E2 and E3 in Table 3 respecitively. Red line is the median value.

Fig. 9 Layouts of the skeletonized systems produced by the proposed TBM-Max for Case 2. (a) E_{tol} = 0.001, skeletonization level is 39.9% (Level 1); (b) E_{tol} = 0.01, skeletonization level is 62.3% (Level 2); and (c) E_{tol} = 1.0, skeletonization level is 67.9% (Level 3)

Fig. 10 Histplot of the demand allocation coefficients for the skeletonized system using TBM-Max with E_{tol} = 1.0 (Level 3)

Fig. 11 Ranking results of the metrics err_{mean} (a, c, e) and err_{ext} (b, d, f) for different skeletonization methods. (a, b), (c, d) and (e, f) are related to the skeletonized systems of Levels 1, 2 and 3, respectively.

Fig. 12 CDF results of the metrics err_{mean} (a, c, e) and err_{ext} (b, d, f) for different skeletonization methods. (a, b), (c, d) and (e, f) are related to the skeletonized systems of Levels 1, 2 and 3, respectively.

Fig. 13 Results of transient pressure traces at different nodes (refer to Fig. 4) in different cases